A Mode Matching Technique For The Seismic Response Of Liquid Storage Tanks Including Soil-Structure Interaction

Tsouvalas, A.; Molenkamp, T.; Canny, Khairina ; Kroon, D.P.; Versluis, Marco; Peng, Y.; Metrikine, A.

DOI
10.47964/1120.9001.18621

Publication date
2020

Document Version
Final published version

Published in
EURODYN 2020 XI International Conference on Structural Dynamics

Available online at www.easdprocedia.org
EASD Procedia EURODYN (2020) 1-14

EASD Procedia

EURODYN 2020
XI International Conference on Structural Dynamics
M. Papadrakakis, M. Fragiadakis, C. Papadimitriou (eds.)
Athens, Greece, 23–26 November 2020

A MODE MATCHING TECHNIQUE FOR THE SEISMIC RESPONSE OF LIQUID STORAGE TANKS INCLUDING SOIL-STRUCTURE INTERACTION

Apostolos Tsouvalas[1], Timo Molenkamp[1], Khairina Canny[2], David Kroon[1], Marco Versluis[2], Yaxi Peng[1], and Andrei V. Metrikine[1]

[1] Delft University of Technology
Faculty of Civil Engineering and Geosciences
Stevinweg 1, 2628 CN Delft, The Netherlands
e-mail: {a.tsouvalas,t.molenkamp,d.p.kroon,y.peng,a.metrikine}@tudelft.nl

[2] Witteveen+Bos Raadgevende ingenieurs B.V.
Leeuwenbrug 8, 7411 TJ Deventer, The Netherlands
e-mail:{khairina.canny,marco.versluis}@witteveenbos.com

Keywords: liquid storage tank, seismic response, soil-structure interaction, fluid-structure interaction, shells

Abstract. *The paper establishes a computationally inexpensive method to deal with the dynamic response of liquid storage tanks subjected to seismic excitation including dynamic soil-structure interaction. The tank is modelled as a thin shell, the stored liquid is described as an inviscid and incompressible fluid and the soil medium is modelled as an elastic continuum. The dynamic response of the tank-liquid-soil system is derived in the frequency domain using dynamic substructuring and mode matching. The tank vibrations are first expressed in terms of the in-vacuo shell modes while the liquid motion is described as a superposition of linear potentials. The soil reaction to the plate of the tank is derived on the basis of a boundary integral formulation with the excitation field being the seismic free-field ground motion. Due to its high computational efficiency, the proposed method is suitable when a large number of simulations is required as is the case in seismic risk analysis. It overcomes the limitations of most mechanical analogues used nowadays, while at the same time maintains an accuracy comparable to that of finite element models within a fraction of the computation time of the latter.*

ISSN:2311-9020
Peer-review under responsibility of the Organizing Committee of EURODYN 2020.
doi: 10.47964/1120.9001.18621

1 INTRODUCTION

The dynamic response of liquid storage tanks subjected to ground excitation has been a subject of continuous research over the past decades [1]. Despite the many modelling techniques available, most models can be classified into two broad categories: Finite Element (FE) models [2] and simplified mechanical analogues with a few degrees of freedom [3, 4].

In a simplified model, the various components of the tank-liquid system are described by point masses, springs and dashpots at certain locations [5]. Such models are useful for engineering purposes since they can prognosticate the base shear force and the overturning moment [6], however, they have certain limitations. First, they provide estimations of the design stresses at the base of the tank alone. Second, when they need to consider shells of non-uniform thickness or dynamic soil-structure interaction, they become needlessly complex, and even though procedures are described in the design codes to incorporate some of these effects [7], these procedures are approximate and cannot always guarantee accurate solutions. On the contrary, when a detailed dynamic analyis is required, FE modelling is often considered. Detailed FE models can overcome most of the limitations of the simpler models described earlier, however, they are computationally expensive and require experienced end users. In addition, the modelling of the unbounded soil domain and the proper inclusion of the seismic excitation remain always a challenge.

To overcome the disadvantages of the aforementioned modelling methods, this paper introduces an alternative method of numerical analysis of the tank-liquid-soil system. By doing so, one can overcome the main disadvantage of the FE models while, at the same time, computational accuracy stays uncompromised. The linear dynamic response of the tank-liquid-soil system is derived in the frequency domain using a mode-matching, dynamic substructuring technique. The substructuring technique, together with the Rayleigh-Ritz method, have been previously employed in [8, 9] for the solution of tank-liquid dynamic problems albeit in the absence of dynamic soil-structure interaction (SSI). In contrast to these earlier works, in this paper the eigenvalue problems are first formulated to obtain the modes of vibration of the tank and the liquid satisfying a set of predefined boundary conditions in an exact manner. Once the vibration modes of the tank and the liquid are determined to within a set of unknown complex-valued coefficients, the latter are obtained by ensuring the kinematic compatibility at the tank-liquid interface and by satisfying the equations of motion of the shell structure subjected to seismic motion. In addition to that, the dynamic reaction of the soil at the bottom side of the plate is considered through a boundary integral formulation in line with Lin et al. [10], thus coupling the tank-liquid system to the soil modelled as a three-dimensional continuum.

The main novelty of the paper lies in the establishment of a computationally inexpensive method to obtain the solution of the fully coupled tank-liquid-soil system subjected to seismic excitation. The computational efficiency stems from the adoption of the dynamic substructuring technique and the fact that for each substructure a standard eigenvalue problem is first solved before the forced response is treated. As will be shown, for low frequency seismic excitations, a few modes usually suffice to reach satisfactory convergence which adds to the computational speed. Furthermore, the solution technique proposed is very efficient and does not require the treatment of the whole coupled problem anew every time one of the substructures alters, i.e. varying liquid volume in the tank or soil composition. Given that, the authors believe that the proposed method is especially useful when a large number of simulations are required as, for example, is the case in seismic risk analyses and probabilistic assessments; cases in which the engineer is usually restricted to the use of simplistic models not capable of capturing all possible

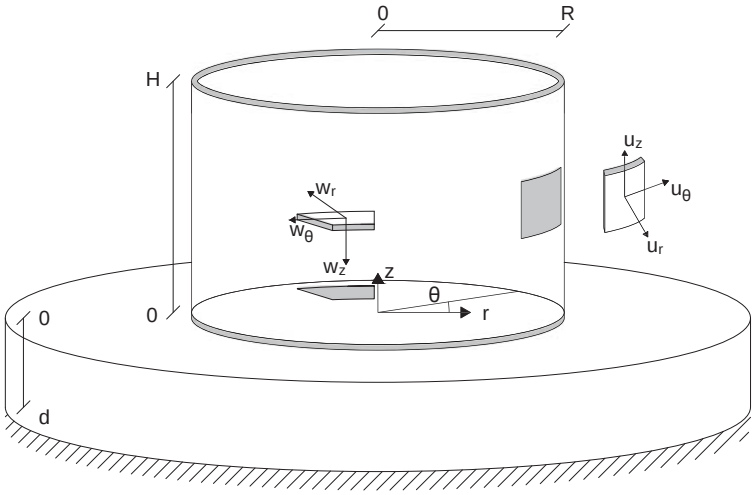

Figure 1: Definition of the displacement components and of the local coordinate system of the tank-liquid-soil system.

failure mechanisms.

In chapter 2, the model is described including the governing equations. The solution method for each subsystem is covered in detail in chapter 3, while chapter 4 establishes the algebraic system of equations that yields the solution to the coupled tank-liquid-soil problem subjected to a seismic excitation. In chapter 5, a convergence analysis is performed and model predictions are compared with FE simulations. Finally, chapter 6, summarises the main results of the paper.

2 MODEL DESCRIPTION

A typical liquid storage tank is shown in Fig.1. The shell structure consists of a circular plate and a cylindrical wall with the parameters E, ν, h and ρ corresponding to the Young's modulus, the Poisson's ratio, the thickness, and the density of the various parts of the shell, respectively. A cylindrical global coordinate system is adopted (r, θ, z) in which r is the radial coordinate, θ is the circumferential coordinate and z is the vertical coordinate. The tank is filled with liquid up to a height of $H_l \leq H$ with H being the height of the wall of the tank. The liquid is assumed inviscid and incompressible with a density ρ_l. The soil column of depth d that supports the tank is modelled as a linear elastic continuum with material parameters ρ_s, λ, μ corresponding to the density and the two Lamè constants of the elastic continuum, respectively. The seismic excitation is included through the free-field ground motion.

The governing equations describing the tank dynamic response read:

$$\boldsymbol{L}_p \boldsymbol{w}_p(r,\theta,t) + \rho_p h_p \ddot{\boldsymbol{w}}_p(r,\theta,t) = \boldsymbol{\sigma}_s(r,\theta,t) + \boldsymbol{p}_p(r,\theta,t) \tag{1}$$

$$\boldsymbol{L}_w \boldsymbol{u}_w(\theta,z,t) + \rho_w h_w \ddot{\boldsymbol{u}}_w(\theta,z,t) = \boldsymbol{p}_w(\theta,z,t) \tag{2}$$

in which $\boldsymbol{w}_p = [w_r, w_\theta, w_z]^{\mathrm{T}}$ is the displacement vector of the mid-surface of the plate, $\boldsymbol{L}_p$ is the stiffness operator of the plate [11], $\boldsymbol{\sigma}_s = [\tau_{rz}, \tau_{r\theta}, \sigma_z]^{\mathrm{T}}$ represents the boundary stress vector induced by the interaction with the soil (including the seismic excitation), and $\boldsymbol{p}_p = [0, 0, p_{liq}]^{\mathrm{T}}$ accounts for the pressure of the stored liquid. Next to that, $\boldsymbol{u}_w = [u_r, u_\theta, u_z]^{\mathrm{T}}$ denote

the displacement of the mid-surface of the wall along the radial, circumferential and vertical directions, respectively. The operator $\boldsymbol{L}_w$ accounts for the stiffness of the cylindrical shell [12] and the force vector $\boldsymbol{p}_w = [p_{liq}, 0, 0]^{\mathrm{T}}$ includes the pressure exerted by the motion of the stored liquid normal to the shell surface. In Eqs.(1–2), the overdot represents a derivative with respect to the time variable.

Supplementary to the equations of motion, a set of boundary and interface conditions need to be formulated to complete the statement of the problem shown in Fig.1:

$$\boldsymbol{u}_w|_{z=0} - \boldsymbol{u}_p|_{r=R} = \boldsymbol{0}\,,\; \phi_{w,z}|_{z=0} - \phi_{p,r}|_{r=R} = 0\,,\; \boldsymbol{f}_w|_{z=0} - \boldsymbol{f}_p|_{r=R} = \boldsymbol{0}\,,\; \boldsymbol{f}_w|_{z=H} = \boldsymbol{0} \tag{3}$$

In Eqs.(3), $\phi_{w,z} = -\partial u_r/\partial z$ and $\phi_{p,r} = -\partial w_z/\partial r$ and $\boldsymbol{f}_w = [M_{zz}, N_{zz}, V_{zr}, T_{z\theta}]^{\mathrm{T}}$ is the generalised force vector of the wall segment which includes the moment M_{zz}, the membrane force N_{zz} and the shear forces V_{zr} and $T_{z\theta}$ [12]. Similarly, $\boldsymbol{f}_p = [M_{rr}, V_r, N_{rr}, N_{r\theta}]^{\mathrm{T}}$ corresponds to the generalised force vector of the plate at the connection with the wall.

Considering a liquid that is inviscid and incompressible, and limiting the scope to linear vibrations, the governing equation for the liquid reads:

$$\nabla^2\phi(r,\theta,z,t) = 0 \tag{4}$$

in which $\phi(r,\theta,z,t)$ denotes the velocity potential. The interface and boundary conditions for the liquid region read:

$$\left.\frac{\partial\phi(r,\theta,z,t)}{\partial r}\right|_{r=R} = \dot{u}_r(\theta,z,t)\,,\; \left.\frac{\partial\phi(r,\theta,z,t)}{\partial z}\right|_{z=0} = \dot{w}_z(r,\theta,t) \tag{5}$$

$$\left.\left(\frac{1}{g}\ddot{\phi}(r,\theta,z,t) - \frac{\partial\phi(r,\theta,z,t)}{\partial z}\right)\right|_{z=H_l} = 0 \tag{6}$$

A single soil layer is considered and the local coordinate system is employed with the z-coordinate pointing downwards, such that the soil surface is at $z = 0$ and the bedrock at $z = d$. The equations of motion read [13]:

$$(\lambda+\mu)\nabla\nabla\boldsymbol{u}_s(r,\theta,z,t) + \mu\nabla\times\nabla\times\boldsymbol{u}_s(r,\theta,z,t) = \rho_s\ddot{\boldsymbol{u}}_s(r,\theta,z,t) \tag{7}$$

in which $\boldsymbol{u}_s = [u_{s,r}, u_{s,\theta}, u_{s,z}]^{\mathrm{T}}$. The boundary conditions and interface conditions of the soil domain at $z = 0$ and $z = d$ read:

$$\begin{array}{rcll} \boldsymbol{u}_s(r,\theta,d,t) & = & \boldsymbol{0} & \\ \boldsymbol{u}_s(r,\theta,0,t) & = & \boldsymbol{u_p}(r,\theta,t) & r \le R \\ \boldsymbol{\sigma}_s^s(r,\theta,0,t) & = & \left\{ \begin{array}{ll} \boldsymbol{0} & r > R \\ -\boldsymbol{K}_s(r,\theta,t) * \left(\boldsymbol{u}_s^f(r,\theta,0,t) - \boldsymbol{u}_p(r,\theta,t)\right) & r \le R \end{array} \right. & \end{array} \tag{8}$$

in which $\boldsymbol{\sigma}_s^s$ is the surface traction acting on the plate along the r-, θ- and z-coordinate at $z = 0$ and the asterisk denotes a convolution operation. The term $\boldsymbol{K}_s(r,\theta,t)$ denotes the dynamic stiffness of the soil column evaluated at the surface of the ground as explained in section 3.3 and $\boldsymbol{u}_s^f(r,\theta,0,t)$ is the free-field ground motion which defines here the excitation mechanism. Equations (1–8) govern the dynamics of the tank-soil-liquid system in the time domain.

3 SOLUTION APPROACH PER SUBSTRUCTURE

The governing equations (1–8) are first transformed to the frequency domain by introducing the Fourier transform pair with respect to time as follows:

$$\tilde{G}(\omega) = \int_{-\infty}^{\infty} g(t)\mathrm{e}^{-\mathrm{i}\omega t}\,\mathrm{d}t \;\text{ and }\; g(t) = \frac{1}{2\pi}\int_{-\infty}^{\infty} \tilde{G}(\omega)\mathrm{e}^{\mathrm{i}\omega t}\mathrm{d}\omega, \tag{9}$$

in which $g(t)$ is understood here as the examined quantity. Complex-valued variables in the frequency domain are indicated with a tilde over the variable.

The resulting set of coupled partial differential equations need to be solved for each excitation frequency. The solution approach is based on the following steps: (i) Solution to the eigenvalue problem of the tank *in-vacuo* (section 3.1); (ii) Eigensolutions of the liquid domain (section 3.2); (iii) Derivation of the dynamic stiffness matrix of the soil at the interface with the tank in the frequency domain (section 3.3); (iv) Solution to the coupled tank-liquid-soil system by making use of the steps (i–iii) as described further in section 4.

3.1 Eigenvalue problem of the tank *in-vacuo*

The equations of motion, boundary and interface conditions for the plate and wall of the tank, neglecting the presence of the water and the soil, are transformed into the frequency domain by means of Eq.(9). The solution is found via separation of variables [14]. A set of algebraic equations is found for the *in-vacuo* shell modes after substituting the assumed solutions for the plate and the wall into the boundary and interface conditions.

$$\boldsymbol{G}_n \cdot \boldsymbol{a} = 0 \tag{10}$$

$\boldsymbol{G}_n$ denotes the coefficient matrix and $\boldsymbol{a}$ is a vector composed of the unknown constants. For a non-trivial solution, the determinant of the coefficient matrix $\boldsymbol{G}_n$ is set equal to zero, i.e. $\det(\boldsymbol{G}_n) = 0$. This results at a transcendental equation which yields an infinite set of eigenvalues ω_{nm} with $m = 0, 1, 2, 3, ...$ for each circumferential order n. A numerical algorithm is developed with the frequency ω (for every circumferential order n) defined as the running variable which is then iterated numerically to find the zeroes of the determinant. Once the values of ω_{nm} are obtained, the tank motion can be expressed as a summation of modes in the frequency domain:

$$\tilde{\boldsymbol{w}}_p(r,\theta,\omega) = \sum_{n=0}^{\infty}\sum_{m=0}^{\infty} \tilde{X}_{nm}\boldsymbol{D}_n^t(\theta)\boldsymbol{W}_{nm}(r) \tag{11}$$

$$\tilde{\boldsymbol{u}}_w(\theta,z,\omega) = \sum_{n=0}^{\infty}\sum_{m=0}^{\infty} \tilde{X}_{nm}\boldsymbol{D}_n^t(\theta)\boldsymbol{U}_{nm}(z) \tag{12}$$

$\boldsymbol{D}_n^t(\theta) = \textit{diag}\ [\cos(n\theta), \sin(n\theta), \cos(n\theta)]$ contains the circumferential dependency of the tank modes and $\boldsymbol{W}_{nm} = [W_{z,nm}, W_{\theta,nm}, W_{r,nm}]^{\mathrm{T}}$ and $\boldsymbol{U}_{nm} = [U_{z,nm}, U_{\theta,nm}, U_{r,nm}]^{\mathrm{T}}$ are the eigenvectors of the plate and the wall, respectively. The indices n, m define the circumferential and axial mode numbers, respectively. The unknown complex-valued amplitudes $\tilde{X}_{nm}$ can be obtained by satisfying the forced vibration problem. The eigenvectors satisfy the following orthogonality condition:

$$\rho_p h_p \iint_S \boldsymbol{D}_q^t\boldsymbol{U}_{ql}^{\mathrm{T}}\boldsymbol{D}_n^t\boldsymbol{U}_{nm}\mathrm{d}S + \rho_w h_w \iint_{S_0} \boldsymbol{D}_q^t\boldsymbol{W}_{ql}^{\mathrm{T}}\boldsymbol{D}_n^t\boldsymbol{W}_{nm}\mathrm{d}S_0 = a_n\Gamma_{nm}\delta_{qn}\delta_{lm}\,, \tag{13}$$

in which δ_{np} and δ_{ml} are the *Kronecker* deltas and S, S_0 denote the surface of integration for the wall and the plate of the tank, respectively. The scalar quantity a_n denotes an integration constant related to the circumference, i.e. $\int_0^{2\pi} D_q^t D_n^t d\theta = a_n \delta_{qn}$; a_n equals π for $n = 0$ and 2π otherwise.

3.2 Eigensolutions of the liquid domain

The liquid potential function is separated into three scalar functions, each one satisfying a subset of the imposed boundary and interface conditions. This allows an analytical treatment of the problem [15]. The total liquid potential is decomposed into three velocity potentials, namely: (i) $\phi^{(1)}(r, \theta, z, t)$ which satisfies the homogeneous boundary conditions at $z = 0$ and $z = H_l$ as well as the imposed kinematic constraint at the interface with the wall; (ii) $\phi^{(2)}(r, \theta, z, t)$ which satisfies the homogeneous boundary conditions at $r = R$ and $z = H_l$, and the imposed kinematic constraint at the interface with the plate; and (iii) $\phi^{(3)}(r, \theta, z, t)$ which does not alter the conditions satisfied already at $z = 0$ and $r = R$ but allows exact satisfaction of the boundary condition at $z = H_l$.

The superposition of the three scalar functions provides the total solution which can be expressed as follows [8]:

$$\tilde{\phi}(r, \theta, z) = \sum_{n=0}^{\infty} \sum_{a=1}^{\infty} \tilde{\phi}_{na}^{(1)} + \tilde{\phi}_{00}^{(2)} + \sum_{n=0}^{\infty} \sum_{b=1}^{\infty} \tilde{\phi}_{nb}^{(2)} + \tilde{\phi}_{00}^{(3)} + \sum_{n=0}^{\infty} \sum_{c=1}^{\infty} \tilde{\phi}_{nc}^{(3)}, \tag{14}$$

in which the following definitions hold:

$$\tilde{\phi}_{na}^{(1)}(r, \theta, z) = \tilde{P}_{na} \phi_{z,na}^{(1)}(z) \phi_{r,na}^{(1)}(r) \cos(n\theta) \tag{15}$$

$$\tilde{\phi}_{00}^{(2)}(r, \theta, z) = \tilde{Q}_{00}(z - H_l) \tag{16}$$

$$\tilde{\phi}_{nb}^{(2)}(r, \theta, z) = \tilde{Q}_{nb} \phi_{z,nb}^{(2)}(z) \phi_{r,nb}^{(2)}(r) \cos(n\theta) \tag{17}$$

$$\tilde{\phi}_{00}^{(3)}(r, \theta, z) = \tilde{S}_{00} \tag{18}$$

$$\tilde{\phi}_{nc}^{(3)}(r, \theta, z) = \tilde{S}_{nc} \phi_{z,nc}^{(3)}(z) \phi_{r,nc}^{(3)}(r) \cos(n\theta) \tag{19}$$

The modal amplitudes $\tilde{P}_{na}$, $\tilde{Q}_{nb}$, and $\tilde{S}_{nc}$ are the unknown complex constants for the liquid domain which will be determined together with the modal amplitudes of the structure by satisfying the forced equations of motion and the kinematic conditions at the tank-liquid interfaces described previously. The index n denotes the circumferential mode number of each potential. The indices a, b and c denote the axial mode numbers. The terms ε_{nb} and ε_{nc} are the roots obtained by setting $J_n'(\varepsilon) = 0$.

3.3 Dynamic stiffness of the soil

To obtain the dynamic stiffness of the soil, the equations are first transformed into the frequency-Hankel domain by means of a Fourier-Hankel transform. In this transformed domain, the dynamic stiffness matrix of a single soil layer reads [13]:

$$\begin{bmatrix} \bar{\boldsymbol{p}}(k, 0) \\ \bar{\boldsymbol{p}}(k, d) \end{bmatrix} = \begin{bmatrix} \bar{\boldsymbol{S}}_{11} & \bar{\boldsymbol{S}}_{12} \\ \bar{\boldsymbol{S}}_{21} & \bar{\boldsymbol{S}}_{22} \end{bmatrix} \begin{bmatrix} \bar{\boldsymbol{u}}(k, 0) \\ \bar{\boldsymbol{u}}(k, d) \end{bmatrix}, \tag{20}$$

in which $\bar{\boldsymbol{p}}(k, 0; d)$, $\bar{\boldsymbol{u}}(k, 0; d)$ correspond to the boundary stress and displacement vectors, respectively, and the bar denotes functions in the frequency-wavenumber domain. The matrix $\bar{\boldsymbol{S}}$

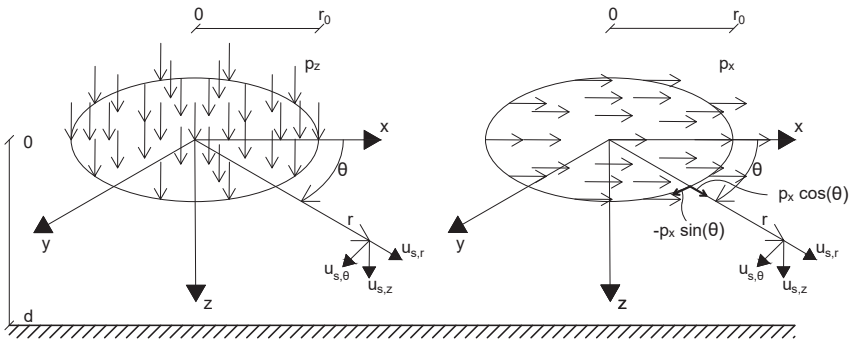

Figure 2: Vertical and horizontal loads distributed evenly over a circular subdisk.

is the dynamic stiffness matrix in the wavenumber-frequency domain. The only terms of interest in $\bar{\boldsymbol{S}}$ are $\bar{\boldsymbol{S}}_{11}$, since the stiffness is needed only at the ground surface. For the sake of brevity of the notations hereafter, we adopt $\bar{\boldsymbol{u}}(k) = \bar{\boldsymbol{u}}(k,0)$, $\bar{\boldsymbol{p}}(k) = \bar{\boldsymbol{p}}(k,0)$ and $\bar{\boldsymbol{p}}(k) = \bar{\boldsymbol{S}}_{11}\bar{\boldsymbol{u}}(k)$. The inverse of the dynamic stiffness matrix of the ground surface, i.e. the flexibility matrix, is of the form:

$$\bar{\boldsymbol{S}}_{11}^{-1} = \bar{\boldsymbol{F}} = \begin{bmatrix} \bar{F}_{11} & 0 & \bar{F}_{13} \\ 0 & \bar{F}_{22} & 0 \\ \bar{F}_{31} & 0 & \bar{F}_{33} \end{bmatrix} \tag{21}$$

Having established a relation between the stresses and displacements at the surface of the ground, one can derive the dynamic stiffness in a straightforward manner. The plate of the tank is assumed to contact the ground surface through circular areas referred to as subdiscs. The loads over a circular subdisk are expanded in Fourier series in the circumferential direction, where $n = 0$ relates to an axisymmetric load and $n = 1$ to an antisymmetric load. The complex amplitudes of the load are related by the following Fourier-Hankel transform pair [13]:

$$\begin{aligned} \bar{\boldsymbol{p}}_n(k) &= a_n \int_{r=0}^{\infty} r\boldsymbol{C}_n(kr) \int_{\theta=0}^{2\pi} \boldsymbol{D}_n(\theta)\tilde{\boldsymbol{p}}(r,\theta)\mathrm{d}\theta\mathrm{d}r \\ \tilde{\boldsymbol{p}}(r,\theta) &= \sum_{n=0}^{\infty} \boldsymbol{D}_n(\theta) \int_{k=0}^{\infty} k\boldsymbol{C}_n(kr)\bar{\boldsymbol{p}}_n(k)\mathrm{d}k \end{aligned} \tag{22}$$

In Eq.(22), a_n is a normalization factor that is equal to $1/2\pi$ or $1/\pi$ for $n = 0$ and $n \neq 0$ respectively. $\boldsymbol{D}_n$ is a diagonal matrix with trigonometric functions, describing the circumferential dependency and $\boldsymbol{C}_n$ contains Bessel functions. Three load cases are considered. A vertical load case and two horizontal load cases; one symmetric and one anti-symmetric with respect to $\theta = 0$. The derivation of the latter two cases is identical but for the trigonometric functions in $\boldsymbol{D}_n$.

The radius of each subdisk equals r_0 and the amplitudes of the vertical and horizontal loads are denoted as p_z and p_x, respectively, as shown in Fig.2. The vertical load, that is assumed uniformly distributed over the subdisc, is transformed into the wavenumber domain by means of Eq.(22):

$$\bar{\boldsymbol{p}}_0(k) = \frac{1}{2\pi} \int_{r=0}^{r_0} r\boldsymbol{C}_0(kr) \int_{\theta=0}^{2\pi} [0,0,p_z]^{\mathrm{T}}\mathrm{d}\theta\mathrm{d}r = -\frac{r_0}{k} J_1(kr_0)[0,0,p_z]^{\mathrm{T}} \tag{23}$$

$\bar{\boldsymbol{p}}_0(k)$ relates to $\bar{\boldsymbol{u}}(k)$ through the flexibility matrix Eq.(21):

$$\bar{\boldsymbol{u}}_0(k) = -\frac{p_z r_0}{k} J_1(kr_0)[\bar{F}_{13},0,\bar{F}_{33}]^{\mathrm{T}} \tag{24}$$

The displacements of the surface at any r and θ are found by:

$$\tilde{\boldsymbol{u}}_s^z(r,\theta) = -r_0 p_z \int_{k=0}^{\infty} J_1(kr_0)\boldsymbol{C}_0(kr)\left[\bar{F}_{13}, 0, \bar{F}_{33}\right]^{\mathrm{T}} \mathrm{dk} \tag{25}$$

Following a similar procedure for the horizontal load one obtains:

$$\tilde{\boldsymbol{u}}_s^x = r_0 p_x \boldsymbol{D}_1(\theta) \int_{k=0}^{\infty} J_1(kr_0)\boldsymbol{C}_1(kr)\left[\bar{F}_{11}, \bar{F}_{22}, \bar{F}_{31}\right]^{\mathrm{T}} \mathrm{dk} \tag{26}$$

Applying the load in y-direction ($\theta = \pi$), via the same steps, an expression can be found similar to Eq.(26).

The integrals in Eqs.(25–26) are evaluated by making use of contour integration. The solution derived holds both within and outside the subdisk. The resulting expressions for $r \leq r_0$ read:

$$\tilde{\boldsymbol{u}}_s^z(r,\theta) = \tilde{p}_z \left(r_0 \pi \mathrm{i} \sum_{k_r} H_1^{(2)}(k_r r_0)\boldsymbol{C}_0(k_r r) \left[\frac{\bar{F}_{13}^n}{\tilde{F}_{p,k}^d}, 0, \frac{\bar{F}_{33}^n}{\bar{F}_{p,k}^d}\right]^{\mathrm{T}} + \left[0, 0, \bar{F}_{33}(0)\right]^{\mathrm{T}} \right), \tag{27}$$

$$\tilde{\boldsymbol{u}}_s^x = -\tilde{p}_x \boldsymbol{D}_1(\theta) \left(r_0 \pi \mathrm{i} \sum_{k_r} H_1^{(2)}(k_r r_0)\boldsymbol{C}_1(k_r r) \left[\frac{\bar{F}_{11}^n}{\bar{F}_{p,k}^d}, \frac{\bar{F}_{22}^n}{\bar{F}_{s,k}^d}, \frac{\bar{F}_{31}^n}{\bar{F}_{p,k}^d}\right]^{\mathrm{T}} - \left[\bar{F}_{11}(0), \bar{F}_{11}(0), 0\right]^{\mathrm{T}} \right) \tag{28}$$

Similarly, the expressions for $r \geq r_0$ read:

$$\tilde{\boldsymbol{u}}_s^z(r,\theta) = r_0 \tilde{p}_z \pi \mathrm{i} \sum_{k_r} J_1(k_r r_0)\boldsymbol{C}_0(k_r r) \left[\frac{\bar{F}_{13}^n}{\bar{F}_{p,k}^d}, 0, \frac{\bar{F}_{33}^n}{\bar{F}_{p,k}^d}\right]^{\mathrm{T}} \tag{29}$$

$$\tilde{\boldsymbol{u}}_s^x = -r_0 \tilde{p}_x \pi \mathrm{i} \boldsymbol{D}_1(\theta) \sum_{k_r} J_1(k_r r_0)\boldsymbol{C}_1(k_r r) \left[\frac{\bar{F}_{11}^n}{\bar{F}_{p,k}^d}, \frac{\bar{F}_{22}^n}{\bar{F}_{s,k}^d}, \frac{\bar{F}_{31}^n}{\bar{F}_{p,k}^d}\right]^{\mathrm{T}} \tag{30}$$

Equations (27–30) define the frequency response functions (FRFs) for a constant distributed force over a circular area with radius r_0. The superscript n here denotes the numerator of the flexibility functions and d the denominator of those; in all cases the derivative of the denominator is taken with respect to k, indicated with subscript k. The FRFs are derived for a single subdisk around the origin. By normalizing the amplitude of the stresses (p_x, p_y, p_z), the dynamic impedance $\tilde{\boldsymbol{R}}_s(r,\theta)$ is obtained which upon inversion yields the dynamic stiffness of the soil $\tilde{\boldsymbol{K}}_s(r,\theta)$.

4 COUPLED TANK-LIQUID-SOIL SYSTEM

The motion of the liquid is described by Eqs.(14–19) and the motion of the tank by Eqs.(11–12). Upon substitution of these expressions into the interface and boundary conditions given by

Eqs.(5–6), and after the use of the orthogonality conditions, one obtains:

$$\Gamma_{na}\tilde{P}_{na} = -\mathrm{i}\omega \sum_{m=0}^{\infty} \tilde{X}_{nm} \int_0^{H_l} \phi^{(1)}_{z,na}(z) U_{r,nm}(z) \mathrm{d}z \tag{31}$$

$$\Gamma_{nb}\tilde{Q}_{nb} = -\mathrm{i}\omega \sum_{m=0}^{\infty} \tilde{X}_{nm} \int_0^{R} \phi^{(2)}_{r,nb}(r) W_{z,nm}(r) r \mathrm{d}r \tag{32}$$

$$\begin{aligned}\Gamma_{nc}\tilde{S}_{nc} = &\sum_{a=1}^{\infty} \tilde{P}_{na} \left.\frac{\partial \phi^{(1)}_{z,na}(z)}{\partial z}\right|_{z=H_l} \int_0^{R} \phi^{(3)}_{r,nc}(r)\phi^{(1)}_{r,na}(r) r \mathrm{d}r \\ &+ \sum_{b=1}^{\infty} \tilde{Q}_{nb} \left.\frac{\partial \phi^{(2)}_{z,nb}(z)}{\partial z}\right|_{z=H_l} \int_0^{R} \phi^{(3)}_{r,nc}(r)\phi^{(2)}_{r,nb}(r) r \mathrm{d}r\end{aligned} \tag{33}$$

The integration constants derived directly from the orthogonality relations are omitted here for the sake of brevity. Next to the satisfaction of the kinematic conditions at the tank-liquid interface, the forced equations of motion of the structure need to be satisfied. Considering Eqs. (11–12) and the fact that for every mode of vibration of the shell $\boldsymbol{L}_w \boldsymbol{u}_{nm} = \omega^2_{nm} \rho_w h_w \boldsymbol{u}_{nm}$ and $\boldsymbol{L}_p \boldsymbol{w}_{nm} = \omega^2_{nm} \rho_p h_p \boldsymbol{w}_{nm}$, the stiffness terms can be replaced by the inertia ones, i.e.:

$$\sum_{n=0}^{\infty}\sum_{m=0}^{\infty} \left(\left(\omega^2_{nm} - \omega^2\right) \rho_p h_p + \tilde{\boldsymbol{K}}_s \right) \tilde{X}_{nm} \boldsymbol{D}^t_n \boldsymbol{W}_{nm} - \tilde{\boldsymbol{p}}_{p,n} \cos(n\theta) = \tilde{\boldsymbol{K}}_s \tilde{\boldsymbol{u}}^f_s \tag{34}$$

$$\sum_{n=0}^{\infty}\sum_{m=0}^{\infty} \left(\omega^2_{nm} - \omega^2\right) \rho_w h_w \tilde{X}_{nm} \boldsymbol{D}^t_n \boldsymbol{U}_{nm} - \tilde{\boldsymbol{p}}_{w,n} \cos(n\theta) = 0 \tag{35}$$

in which the liquid pressures are $\tilde{\boldsymbol{p}}_{n,p} = [0, 0, \tilde{p}_{n,l}|_{z=0}]^{\mathrm{T}}$ and $\tilde{\boldsymbol{p}}_{n,w} = [\tilde{p}_{n,l}|_{r=R}, 0, 0]^{\mathrm{T}}$. $\boldsymbol{W}_{nm}$ and $\boldsymbol{U}_{nm}$ are the eigenvectors of the plate and wall respectively with respect to circumferential mode number n and axial mode number m. By substituting Eqs.(15–19) into $\tilde{\boldsymbol{p}}_{n,p}$ and $\tilde{\boldsymbol{p}}_{n,w}$ one can expand the liquid pressures in terms of the summation of the potential functions. By summing up the components of Eqs.(34–35), one can make use of Eq.(13) to eliminate part of the modal summations. By considering the above, the final set of infinite equations that needs to be solved for every n-mode number reads:

$$\begin{aligned}\sum_{m=0}^{\infty} \left(\omega^2_{nm} - \omega^2\right) \Gamma_{nm} - \int_0^{R} \boldsymbol{W}^{\mathrm{T}}_{nm} \tilde{\boldsymbol{p}}_{p,n} \mathrm{d}r - \int_0^{H} \boldsymbol{W}^{\mathrm{T}}_{nm} \tilde{\boldsymbol{p}}_{w,n} \mathrm{d}z \\ = \frac{1}{a_n} \iint_{S_0} \boldsymbol{D}^t_n \boldsymbol{W}^{\mathrm{T}}_{nm} \tilde{\boldsymbol{K}}_s \left(\tilde{\boldsymbol{u}}^f_s - \tilde{X}_{nm} \boldsymbol{D}^t_n \boldsymbol{W}_{nm} \right) \mathrm{d}S_0\end{aligned} \tag{36}$$

This approach is valid as shown in [16] for a pile foundation embedded into the soil. The final matrix equation can be represented in a condensed form as follows:

$$\boldsymbol{Q}_n \cdot \boldsymbol{c}_n = \boldsymbol{F}_n \tag{37}$$

$\boldsymbol{Q}_n$ is the modal coefficient matrix of dimensions $(a+b+c+m) \times (a+b+c+m)$ which is fully-populated, complex-valued, and gathers the multipliers of the amplitude coefficients resulting from equations (31–33) and (36). Vector $\boldsymbol{c}_n$ contains the liquid unknowns P_{na}, Q_{nb}, S_{nc} and modal amplitude coefficients of the structure X_{nm} and is of size $(a + b + c + m)$. Vector $\boldsymbol{F}_n$ represents the modal projection of the dynamic loading. By following a straightforward matrix operation, i.e. $\boldsymbol{c}_n = \boldsymbol{Q}^{-1}_n \boldsymbol{F}_n$, one can obtain both the liquid and the structure unknown constants once a proper truncation scheme of the infinite system is established.

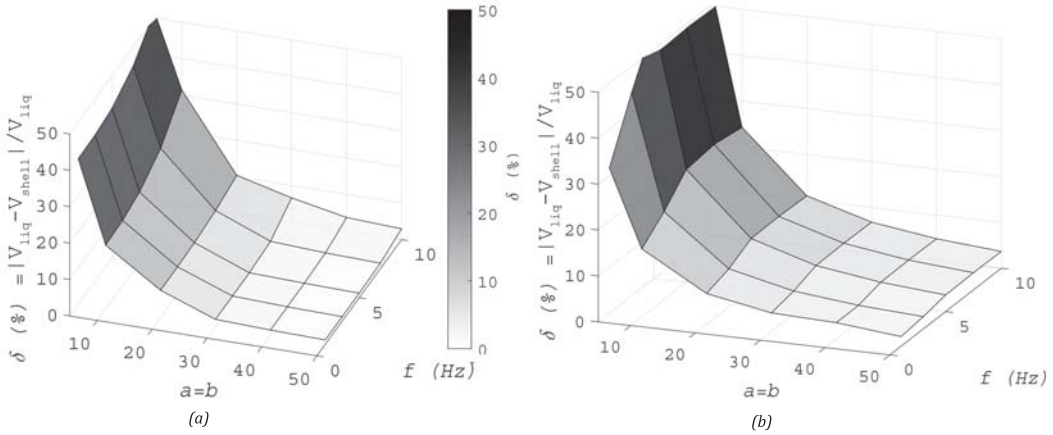

Figure 3: Convergence of the solution for increasing number of axial mode numbers of the liquid domain ($a = b = c$) for: (a) $n = 0$; and (b) $n = 1$.

5 MODEL VALIDATION

The tank-liquid system is validated with a FE model using a Kelvin-Voigt foundation with frequency independent springs and dashpots to represent the SSI effects. The soil domain is validated separately by comparing the results of a harmonically excited rigid massless plate [17, 18].

5.1 Convergence criteria and eigenvalues of the liquid-tank system

The base case considered for validation is a tank with $H/R = 0.71$ and $H = 22$m. The tank is composed of steel material ($\nu = 0.30$ and $\rho = 7850$ kg m^{-3}) with a plate thickness of $h_w = 19$mm and $h_w/h_p = 1.267$. The plate rests on elastic foundation with $k_v = 40$MNm^{-2} and $k_v/k_h = 16$. The stored liquid has a density of 1000kgm^{-3} and a fill level ratio $H_l/H = 1.0$. The adopted computational method involves the truncation of the infinite set of algebraic equations to obtain the unknown modal coefficients. It has been found that the results are most sensitive to the truncation limits of the liquid modes and rather insensitive to the number of structural modes considered as long as a reasonable criterion is adopted for the latter. The number of structural modes to be considered can be estimated by examining the energy spectrum of the dynamic excitation and choosing a truncation limit for the structural modes such that the eigenfrequency of the upper limit in the summation is twice as high as the highest frequency of interest-based on the energy spectrum [19]. Figure 3 depicts the average error at the shell-liquid interface for varying number of liquid modes and for a range of frequencies for two cases of circumferential mode numbers, i.e. $n = 0$ and $n = 1$. As can be seen, when the number of axial modes increases for a given circumferential order, the error decreases monotonically. For the case study considered here, about 30 modes suffice to reduce the error to below 5% for $n = 0$ and about 40 modes to stay within the same limit for $n = 1$.

The proposed model is validated against results obtained by FEM simulations in Comsol Multiphysics® COMSOL Multiphysics® [20]. The validation is performed for several key parameters; here results are shown for a varying liquid volume. As can be seen in Table 1, the differences in the computed eigenvalues between the present model and the FEM are less than 10% in all cases and in most cases below 5%. In Fig. 4, a few mode shapes obtained with the two models are shown. As can be seen, the modes are very similar which proves the validity of the developed model.

$\mathbf{n=1}$	**Present model**		**FEM [20]**		$\lvert\delta f\rvert$ **[%]**	
H_l/H	$f_{1,1}(Hz)$	$f_{1,2}(Hz)$	$f_{1,1}$	$f_{1,2}(Hz)$	$\delta f_{1,1}$	$\delta f_{1,2}$
0%	6.29	12.06	6.42	12.14	2.00	0.63
50%	2.65	6.35	2.39	6.07	9.97	4.55
100%	1.31	3.99	1.24	3.70	5.52	5.80

Table 1: Eigenvalues (in Hertz) obtained by using a FE model in COMSOL Multiphysics® [20] and the present model for the $n = 1$ family of modes and for varying fill height of the liquid.

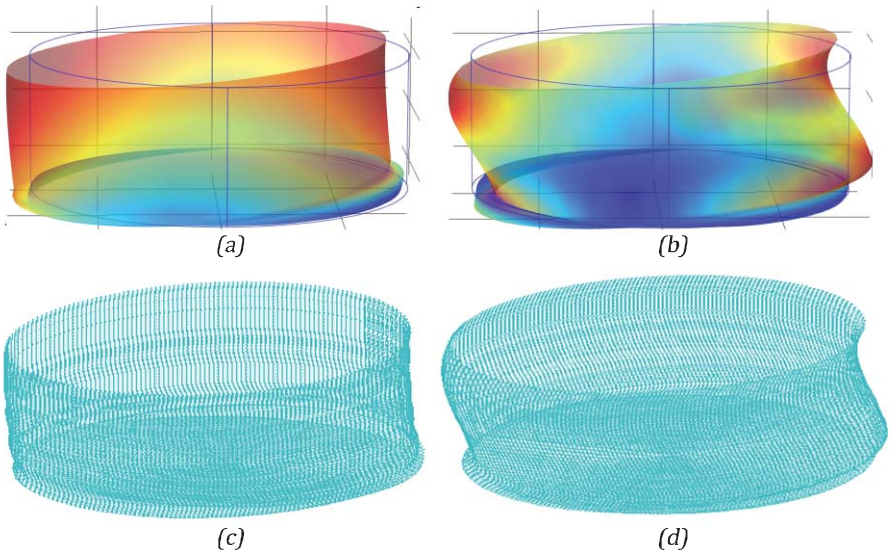

Figure 4: Comparison of the modal shapes of the tank-liquid system obtained by using the FE model in COMSOL Multiphysics® [20] and the present model for a filled tank:(a) FE mode $(1, 1)$; (b) FE mode $(1, 2)$ (c) present model mode $(1, 1)$; (d) present model mode $(1, 2)$.

5.2 Dynamic soil stiffness

The derivation of the dynamic stiffness is benchmarked against results presented in the literature for the case of a rigid plate. To facilitate a direct comparison with literature, a normalized frequency is introduced as $a_0 = \omega R/2\pi c_s$. The dynamic stiffness and damping coefficients in the horizontal direction are defined as:

$$\tilde{K}_{xx} = K^0_{xx}\left(k_{xx} + \mathrm{i}\frac{\omega R}{c_s}c_{xx}\right)(1 + 2\mathrm{i}\beta) \tag{38}$$

in which K^0_{xx} is the static stiffness and k_{xx}, c_{xx} denote the dynamic stiffness and damping coefficients, respectively, and c_s denotes the shear wave speed in the soil.

For the validation case the following values are chosen: $d/R = 2; 4$, $\nu = 1/3$, damping ratio $\beta = 5\%$. The comparison is based on a discretisation of the plate surface in 15 rings yielding in total 709 subdisks. Figure 5 shows that the dynamic stiffness k_{xx} and damping coefficients c_{xx} are in very good agreement with literature [17, 18]. Moreover, the solution for the static case converges relatively fast as shown in Fig.6. It is expected that this is an extreme case since peak stresses are located at the edge of the plate. The subdisks have only one node; thus, the more elements included, the better the stress representation at the edge. When travelling waves with short wavelengths compared to the plate radius are excited, a higher number of elements might be required, albeit in the field of earthquake engineering this is not expected.

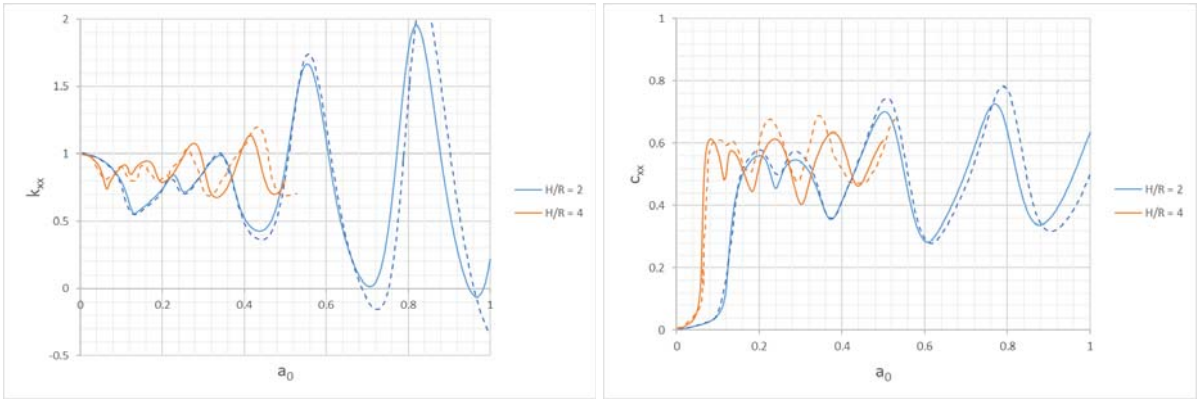

(a) Horizontal stiffness coefficient (b) Horizontal damping coefficient

Figure 5: Comparison of model results (solid lines) and references (dashed lines) [17, 18].

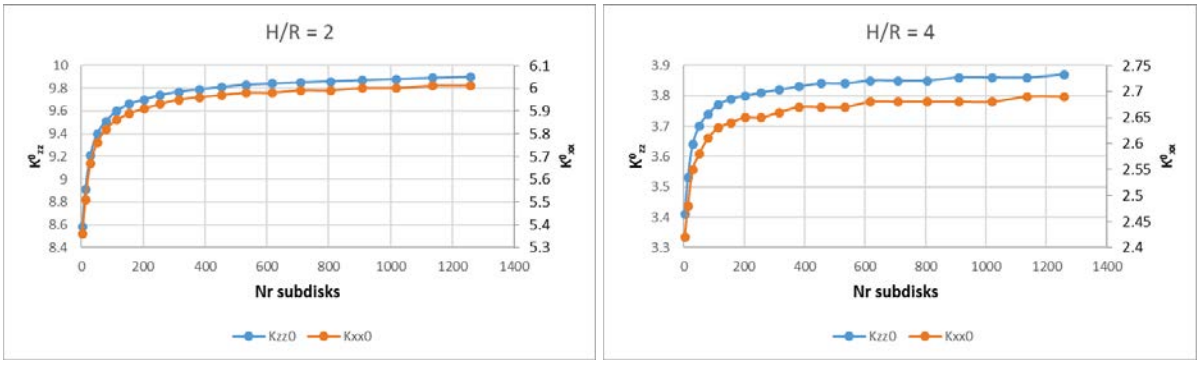

Figure 6: Convergence of the static stiffness for d/R = 2 and d/R = 4.

6 CONCLUSIONS

A computationally inexpensive method is developed for the prediction of the dynamic response of a liquid storage tank subjected to seismic excitation. The model consists of three main subsystems, namely: the shell structure representing the tank, the stored liquid and the soil domain. Emphasis is placed on the theoretical development of the model and the description of an elegant method of solution to the final system of coupled differential equations. The strength of the method is that it can cope with a full dynamic analysis of a coupled tank-liquid-soil system and it can easily be expanded in cases of non-uniform shell thickness and multi-layered soils. Next to that, due to the fact that substructuring forms the basis of the solution technique, the model is suitable for a large number of computations in which some parts of the total system are altered whereas others remain unchanged. The authors believe that the proposed model can be especially useful when a large number of simulations is required as, for example, is the case in seismic risk analyses.

REFERENCES

[1] F. G. Rammerstorfer, K. Scharf, and F. D. Fisher. Storage Tanks Under Earthquake Loading. *Applied Mechanics Reviews*, 43:261–282, 2008.

[2] L. Zhou, Y. Fan, B. Gao, and X. Wang. Seismic response analysis of LNG storage tank

under the vertical earthquake excitation. *Applied Mechanics and Materials*, pages 1743–1746, 2013.

[3] G. W. Housner. The dynamic behavior of water tanks. *Bulletin of the Seismological Society of America*, 53(2):381–387, 1963.

[4] P. K. Malhotra, T. Wenk, and M. Wieland. Simple procedure for seismic analysis of liquid-storage tanks. *Structural Engineering International*, 10(3):197–201, 2000.

[5] G. C. Drosos, A. A. Dimas, and D. L. Karabalis. Discrete Models for Seismic Analysis of Liquid Storage Tanks of Arbitrary Shape and Fill Height. *Journal of Pressure Vessel Technology*, 130(4), 09 2008. ISSN 0094-9930. 041801.

[6] I. P. Christovasilis and A. S. Whittaker. Seismic analysis of conventional and isolated LNG tanks using mechanical analogs. *Earthquake Spectra*, 24:599–616, 2008.

[7] European Commitee for Standardization. EN 1998-4:2006 - Eurocode 8: Design of structures for earthquake resistance - Part 4: Silos, tanks and pipelines. *Eurocode 8: Desing of structures for earthquake resistance*, 4(2006):84, 2006.

[8] M. Amabili. Ritz method and substructuring in the study of vibration with strong fluid-structure interaction. *Journal of Fluids and Structures*, 11:507–523, 1997.

[9] M. Amabili, M. P. Paidoussis, and A. A. Lakis. Vibrations of partially filled cylindrical tanks with ring-stiffeners and flexible bottom. *Journal of Sound and Vibration*, 213:259–299, 1998.

[10] Gao Lin, Zejun Han, and Jianbo Li. An efficient approach for dynamic impedance of surface footing on layered half-space. *Soil Dynamics and Earthquake Engineering*, 49: 39–51, 2013. ISSN 02677261.

[11] A.W. Leissa. *Vibration of Plates*. NASA SP. Scientific and Technical Information Division, National Aeronautics and Space Administration, 1969.

[12] W. Soedel. *Vibrations of Shells and Plates*. McGraw-Hill professional engineering: Mechanical engineering. M. Dekker, 1981. ISBN 9780824711931.

[13] J. P. Wolf. *Dynamic soil-structure interaction*. Prentice-Hall, Englewood Cliffs, 1985. ISBN 0-13-221565-9.

[14] A. Tsouvalas and A. V. Metrikine. Seismic response of the outer shell of a liquefied natural gas storage tank using a semi-analytical dynamic substructuring technique. *International Journal of Earthquake and Impact Engineering*, 1(1-2):98–130, 2016.

[15] J. Habenberger. Fluid damping of cylindrical liquid storage tanks. *SpringerPlus*, 4(1):515, 2015. ISSN 2193-1801.

[16] A. Tsouvalas and A.V. Metrikine. A three-dimensional vibroacoustic model for the prediction of underwater noise from offshore pile driving. *Journal of Sound and Vibration*, 333(8):2283 – 2311, 2014. ISSN 0022-460X.

[17] J. L. Tassoulas. *Elements for the numerical analysis of wave motion in layered media*. Ph.d. thesis, Massachusetts Institute of Technology, 1981.

[18] A. Pais and E. Kausel. Approximate formulas for dynamic stiffnesses of rigid foundations. *Soil Dynamics and Earthquake Engineering*, 7(4):213 – 227, 1988. ISSN 0267-7261.

[19] A. Tsouvalas, K. N. van Dalen, and A. V. Metirikne. The significance of the evanescent spectrum in structure-waveguide interaction problems. *The Journal of the Acoustical Society of America*, 138(4):2574–2588, 2015.

[20] COMSOL Multiphysics®. *www.comsol.com*. Stockholm, Sweden, 2015.